Electric and Velocity Field Determination in the Solar Atmosphere

George H. Fisher,
University of California, Berkeley

Collaborators: Brian Welsch (UCB), Yan Li (UCB), Pete Schuck (NASA/GSFC), Bill Abbett (UCB), Dave Bercik (UCB)

Electric fields on the solar surface determine the flux of magnetic energy and relative magnetic helicity into flare and CME-producing parts of the solar atmosphere:

$$\frac{\partial E_M}{\partial t} = \iint_S dS\, \hat{\mathbf{n}} \cdot \frac{c}{4\pi} \mathbf{E} \times \mathbf{B} \cong \iint_S dS\, \hat{\mathbf{n}} \cdot \frac{-1}{4\pi} (\mathbf{v} \times \mathbf{B}) \times \mathbf{B},$$

$$\frac{\partial E_F}{\partial t} \cong \frac{1}{4\pi} \iint_S dS\, B_n \mathbf{u}_h \cdot (\mathbf{B}_h^{(P)} - \mathbf{B}_h), \text{ where } B_n \mathbf{u}_h \equiv (\mathbf{v}_h B_n - \mathrm{v}_n \mathbf{B}_h),$$

$$\frac{dH}{dt} = 2 \iint_S dS\, \hat{\mathbf{n}} \cdot \mathbf{A_p} \times \mathbf{E} \cong 2 \iint_S dS \left\{ (\mathbf{A_P} \cdot \mathbf{B_h}) \mathrm{v}_n - (\mathbf{A_P} \cdot \mathbf{v_h}) B_n \right\}.$$

Here, $\partial E_M / \partial t$ is the change in magnetic energy in the solar atmosphere, $\partial E_F / \partial t$ is the difference between the rate of change of total magnetic energy and the potential-field magnetic energy, given a surface distribution of $\mathbf{U}_h$ (Welsch 2006, ApJ 638, 1101), and dH/dt is the change of magnetic helicity of the solar atmosphere.

The flow field **v** is important because to a good approximation, **E** =-**v**/c x **B** in the layers where the magnetic field is measured. Here **E** is the electric field, **B** is the magnetic field, and $\mathbf{A_p}$ is the vector potential of the potential magnetic field that matches its measured normal component.

Approaches to Computing Electric Fields from Magnetograms:

- Assume **E**=-**v**/cx**B** and find v from local correlation tracking techniques applied to changes in line-of-sight magnetograms (e.g. FLCT method of Fisher & Welsch) (approach used in 1st part of this talk)
- Use vector magnetograms and normal component of induction equation to determine 3 components of **v** (e.g. ILCT method of Welsch et al (2004), MEF method of Longcope (2004), and DAVE4VM (Schuck 2008)
- Use vector magnetograms to solve all 3 components of the induction equation (2nd part of this talk)

What can we do with time-sequences of line-of-sight magnetograms? (there are currently many more of these than vector magnetograms)

- Compute flow velocity estimates for a moderate sample of active regions as they rotate across the solar disk, using FLCT[1] (Fisher & Welsch 2008), and DAVE[2] (Schuck 2006)
- Compare magnetic field and flow velocity diagnostics with solar flare energy output
- Try to quantify and understand the empirical relationships between flow properties and flare energy output.

[1] FLCT code link: http://solarmuri.ssl.berkeley.edu/~fisher/public/software/FLCT/C_VERSIONS/

[2] DAVE code link: http://wwwppd.nrl.navy.mil/whatsnew/dave/index.html

Fourier local correlation tracking (FLCT) finds **v**(x, y) by correlating subregions, to find local shifts.

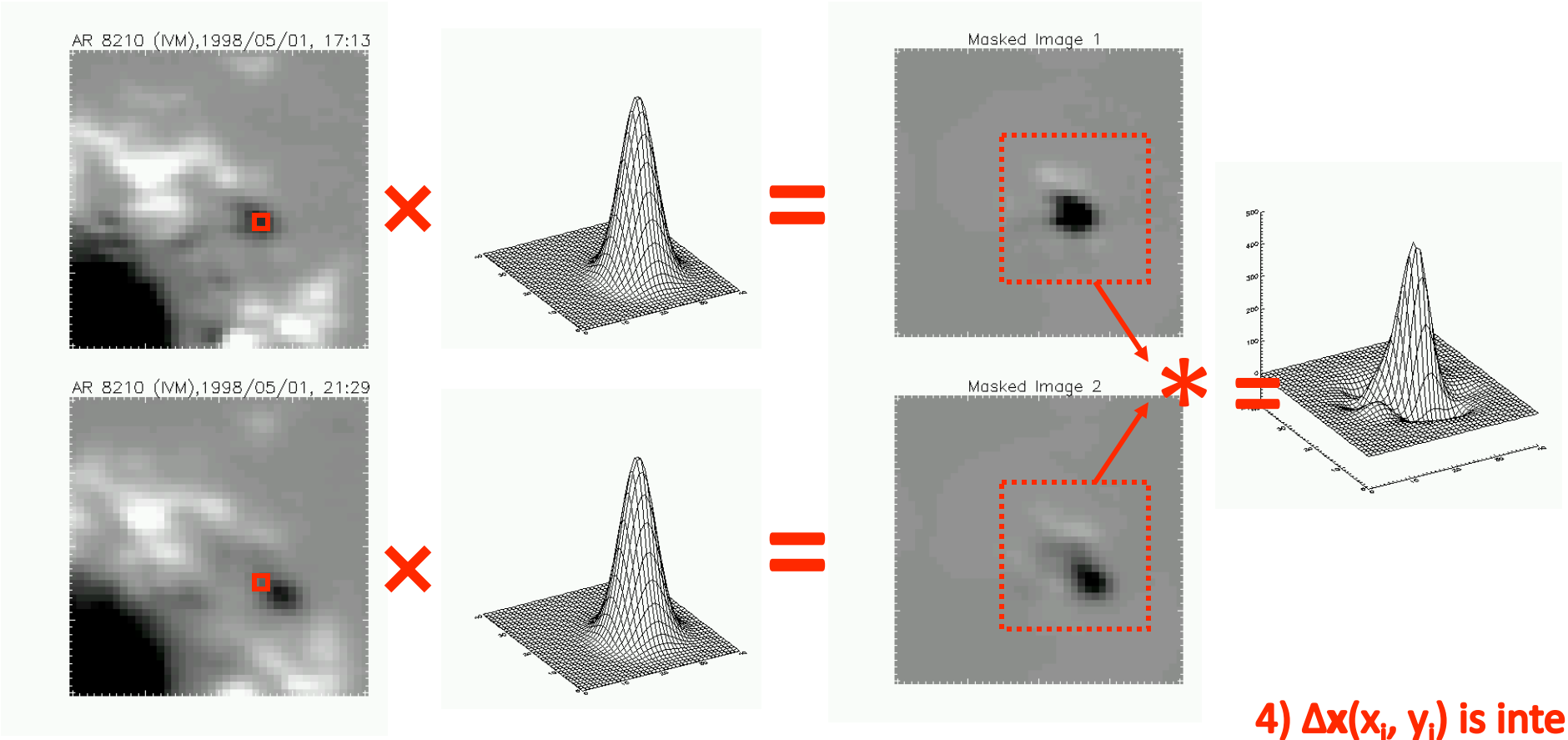

1) for ea. (x_i, y_i) above $|B|_{threshold}$

2) apply Gaussian mask at (x_i, y_i)

3) truncate and cross-correlate

4) $\Delta x(x_i, y_i)$ is inter-polated max. of correlation funct

Example of usage of FLCT

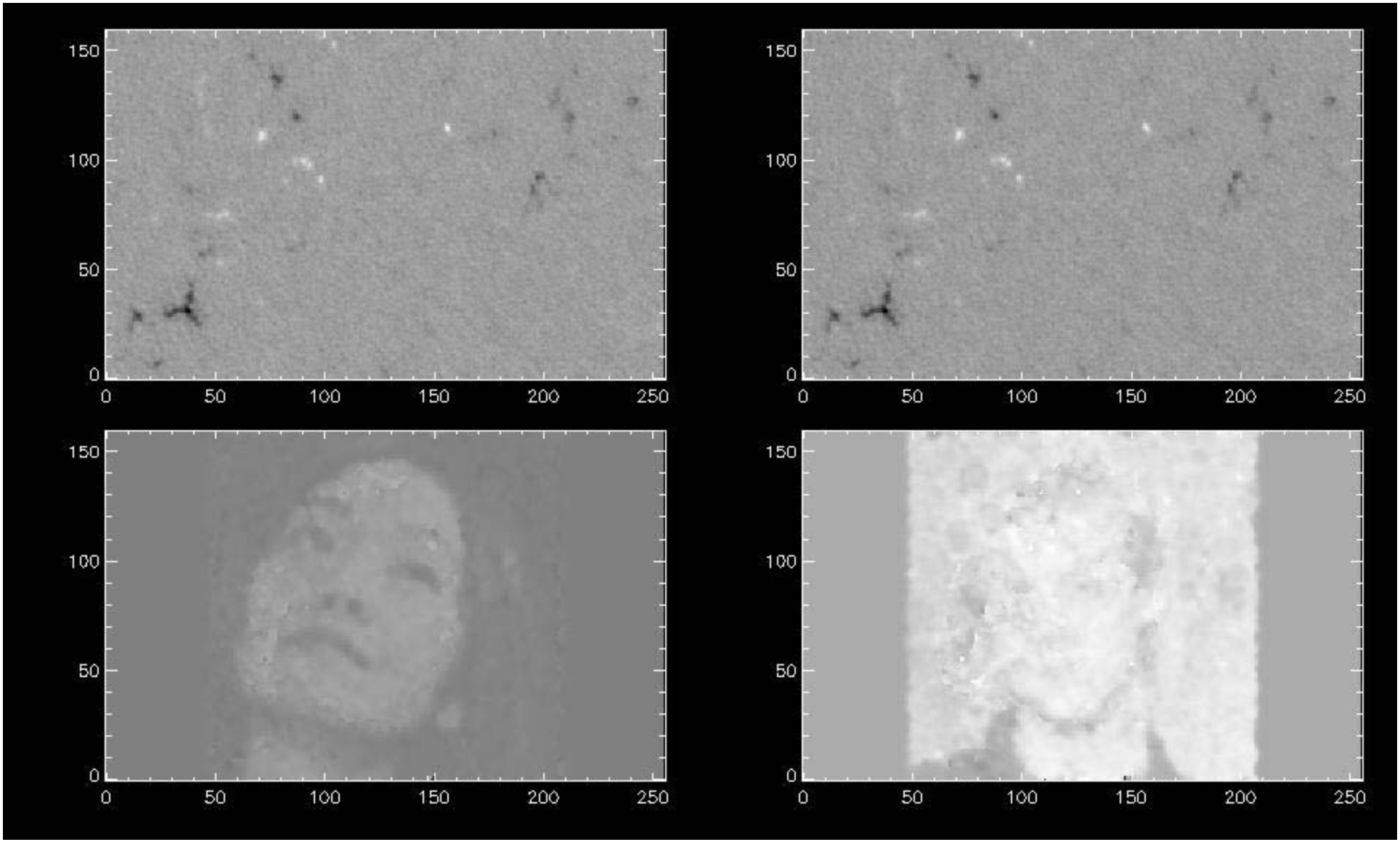

Magnetogram Data Handling

- Pixels > 45° from disk center were not tracked.
- To estimate the radial field, cosine corrections were used, $B_R = B_{LOS}/\cos(\boldsymbol{\Theta})$
- Mercator projections were used to conformally map the irregularly gridded $B_R(\vartheta,\varphi)$ to a regularly gridded $B_R(x,y)$.
- Corrections for scale distortion were applied.

FLCT and DAVE flow estimates were correlated, but differed substantially.

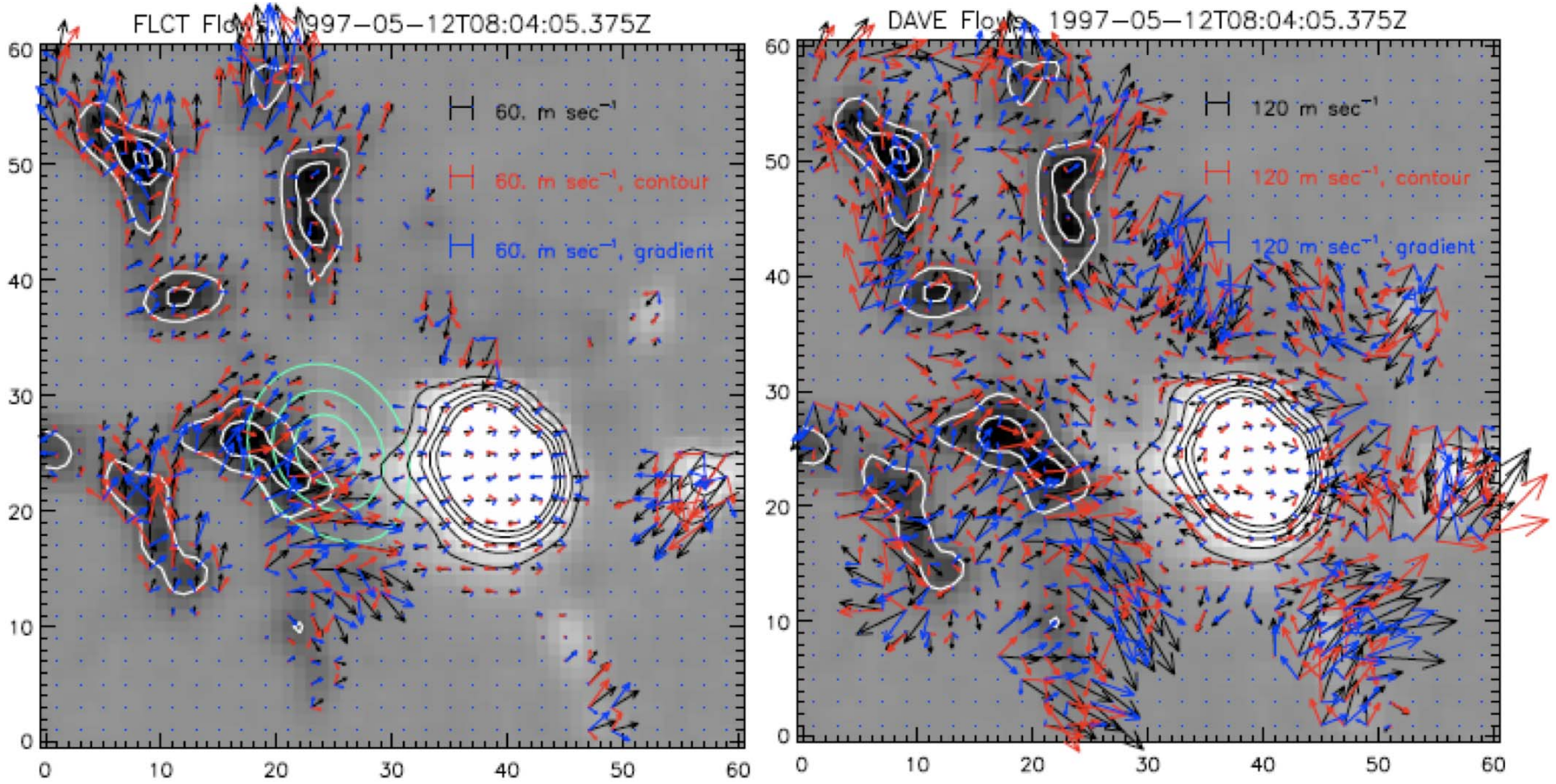

FLCT and DAVE flow estimates were correlated, but differed substantially.

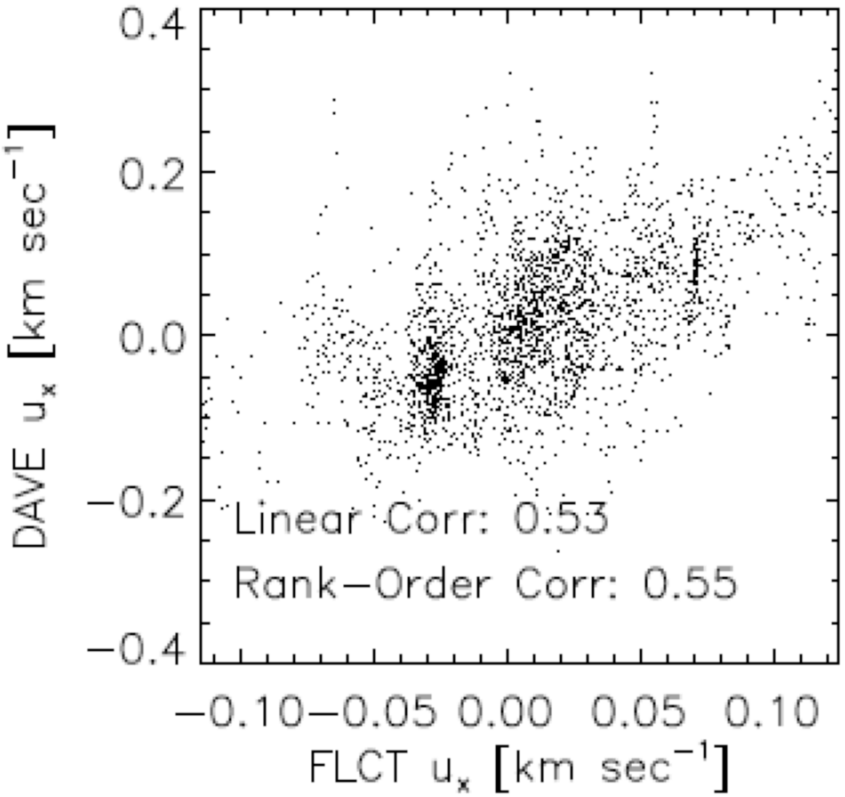

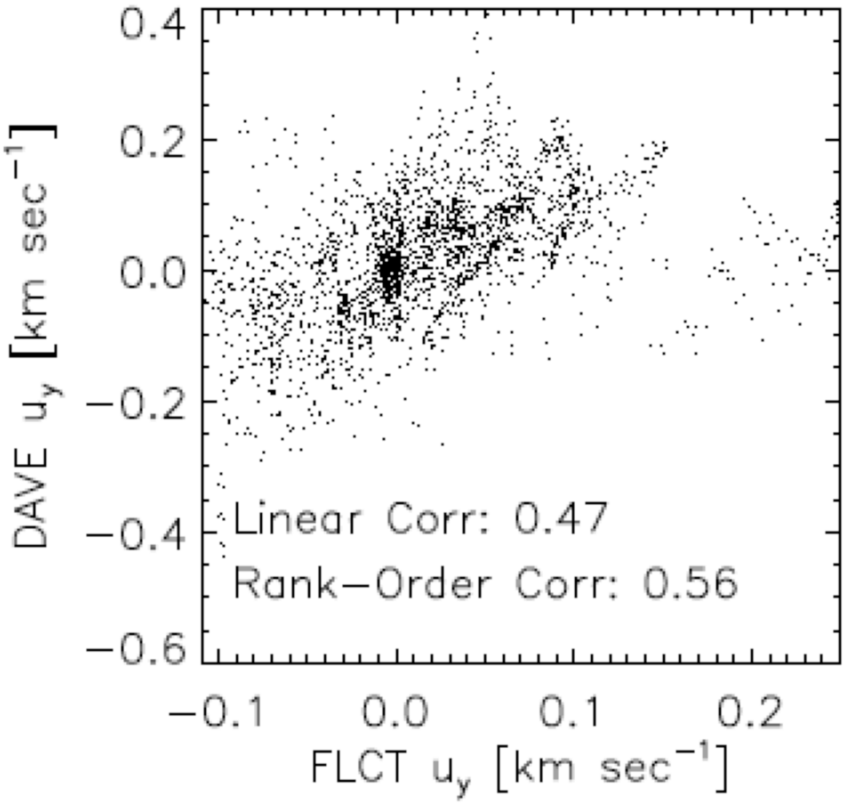

For some ARs in our sample, we auto-correlated u_x, u_y, and B_R, for both FLCT and DAVE flows.

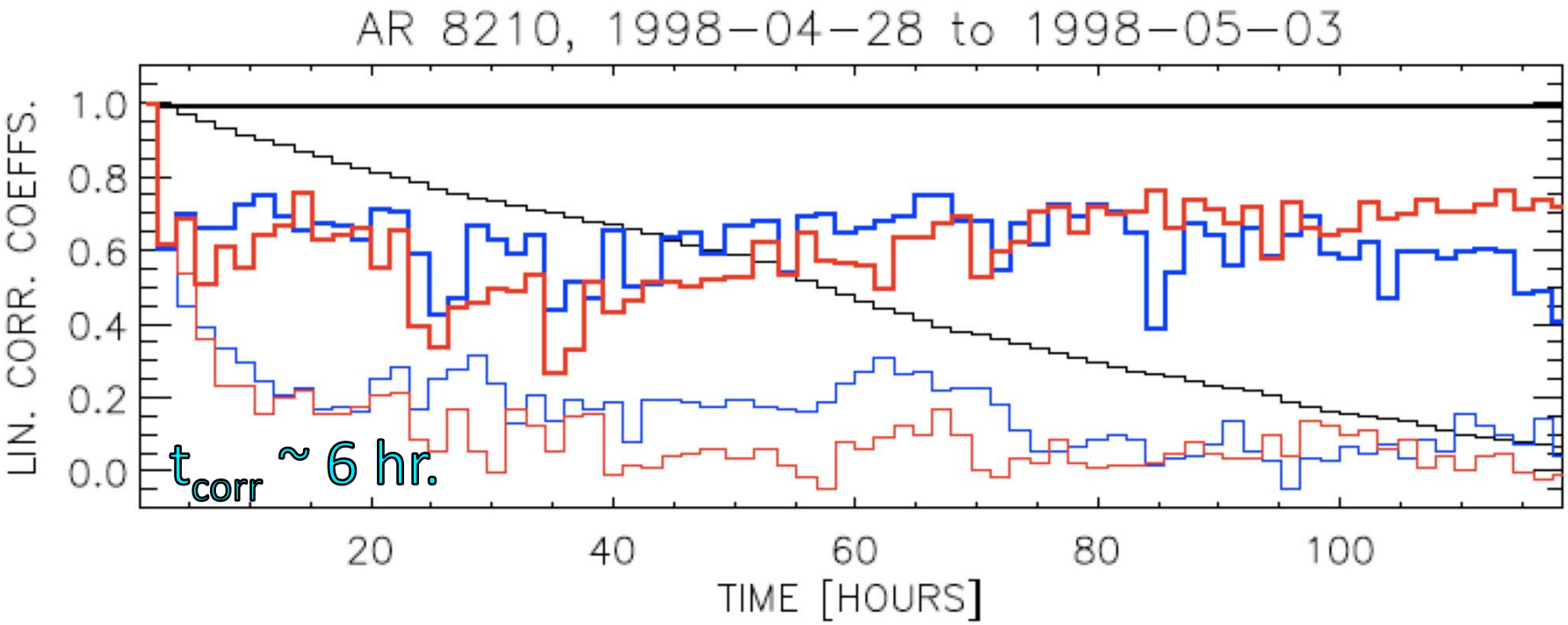

BLACK shows autocorrelation for B_R; **thick** is current-to-previous, thin is current-to-initial.

BLUE shows autocorrelation for u_x; **thick** is current-to-previous, thin is current-to-initial.

RED shows autocorrelation for u_y; **thick** is current-to-previous, thin is current-to-initial.

Parametrization of Flare Productivity

- We binned flares in five time intervals, τ:
  - time to cross the region within 45^{o} of disk center;
  - 6C/24C: the 6 & 24 hr windows centered each flow estimate;
  - 6N/24N: the "next" 6 & 24 hr windows after 6C/24C

- Following Abramenko (2005), we computed an average GOES flare flux [μW/m^2/day] for each window:

$$F = (100\, S^{(X)} + 10\, S^{(M)} + 1.0\, S^{(C)})/\tau\ ;$$

exponents are summed in-class GOES significands

- Our sample: 154 C-flares, 15 M-flares, and 2 X-flares

Correlation analysis showed several variables associated with flare flux *F*. This plot is for disk-passage averaged properties.

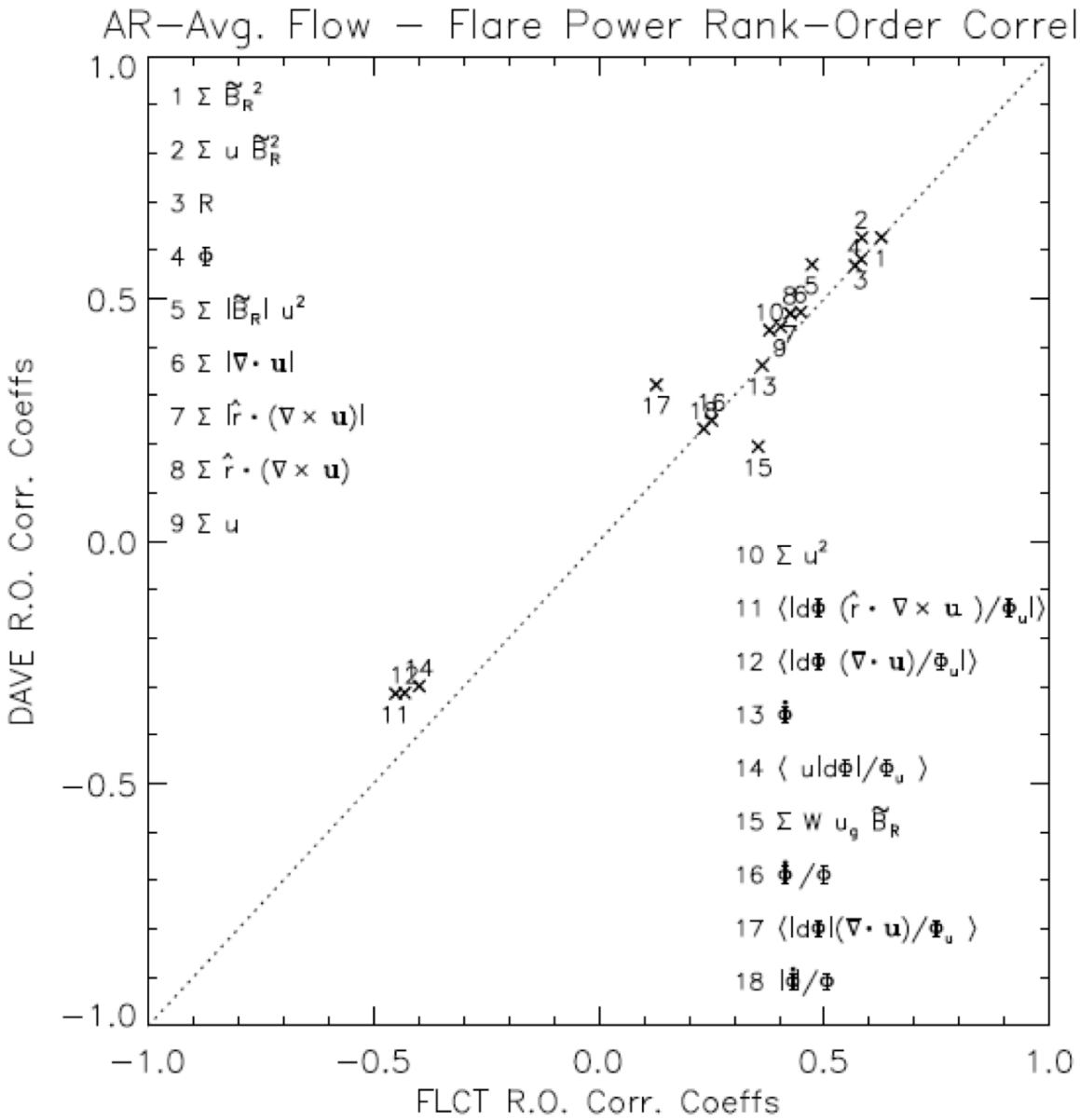

Field and flow properties are ranked by distance from (0,0), complete lack of correlation.

Only the highest-ranked properties tested are shown.

The more FLCT and DAVE correlations agree, the closer they lie to the diagonal line (not a fit).

No purely intensive quantities appear --- all contain extensive properties.

With 2-variable discriminant analysis (DA), we paired $\Sigma\, u\, B_R^2$ "head to head" with each other field/ flow property.

Wind.	Variable(s) Considered[a] [Disc. Coeff.]	PF/F[b]	PNF[c] /F	PF/NF[d]	PNF/NF	*SS*
6C	$\sum u\lvert\tilde{B}_R\rvert^2$	115	201	96	2296	0.16
6C	$\sum u\lvert\tilde{B}_R\rvert^2$ [1.25], R [1.12]	107	209	64	2328	0.20
6C	$\sum u\lvert\tilde{B}_R\rvert^2$ [0.95], R [1.11], $\langle\lvert\tilde{B}_R\rvert\rangle$ [0.39]	108	208	66	2326	0.21
6N	R	39	80	62	2527	-0.08
6N	R [1.96], $\sum u\lvert\tilde{B}_R\rvert^2$ [0.78]	41	78	65	2524	-0.08
6N	R [1.89], $\sum u\lvert\tilde{B}_R\rvert^2$ [0.76], $\dot{R}$ [0.53]	40	79	63	2526	-0.04
24C	$\sum u\lvert\tilde{B}_R\rvert^2$	302	371	74	1961	0.33
24C	$\sum u\lvert\tilde{B}_R\rvert^2$ [1.28], $\langle\lvert\tilde{B}_R\rvert\rangle$ [0.96]	336	337	70	1965	0.37
24C	$\sum u\lvert\tilde{B}_R\rvert^2$ [1.53], $\langle\lvert\tilde{B}_R\rvert\rangle$ [0.88], $\langle\tilde{B}_R\rangle$ [0.48]	354	319	81	1954	0.39
24N	$\sum u\lvert\tilde{B}_R\rvert^2$	118	210	98	2282	0.16
24N	$\sum u\lvert\tilde{B}_R\rvert^2$ [1.43], R [0.67]	115	213	82	2298	0.18
24N	$\sum u\lvert\tilde{B}_R\rvert^2$ [1.45], R [0.40], $\mathcal{F}_{24,\mathrm{current}}$ [0.46]	121	207	72	2308	0.20

For all time windows, regardless of whether FLCT or DAVE flows were used, DA consistently ranked $\Sigma\, u\, B_R^2$ among the two most powerful discriminators.

Summary of Flows/Flares Study

We found $\Sigma\, u\, B_R^2$ and R to be strongly associated with avg. flare flux and flare occurrence.

$\Sigma\, u\, B_R^2$ seems to be a robust predictor:

- speed u was only weakly correlated with B_R;
- $\Sigma\, B_R^2$ was also tested;
- using u from either DAVE or FLCT gave the same result.

This study suffers from low statistics, so further study with larger datasets is needed. (A proposal to extend this work is being written)

This work has been submitted (Welsch, Li, Schuck & Fisher 2009, ApJ).

A copy of the manuscript can be downloaded here:

http://solarmuri.ssl.berkeley.edu/~welsch/public/manuscripts/ms_20090427.pdf

Can we determine the 3D electric field from vector magnetograms?

$$\frac{\partial B_x}{\partial t} = c\left(\frac{\partial E_y}{\partial z} - \frac{\partial E_z}{\partial y}\right)$$

$$\frac{\partial B_y}{\partial t} = c\left(\frac{\partial E_z}{\partial x} - \frac{\partial E_x}{\partial z}\right)$$

$$\frac{\partial B_z}{\partial t} = c\left(\frac{\partial E_x}{\partial y} - \frac{\partial E_y}{\partial x}\right)$$

Kusano et al. (2002, ApJ 577, 501) stated that only the equation for the normal component of B (B_z) can be constrained by sequences of vector magnetograms, because measurements in a single layer contain no information about vertical derivatives. Nearly all current work on deriving flow fields or electric fields make this same assumption. **But is this statement true?**

The magnetic induction equation

Use the poloidal-toroidal decomposition of the magnetic field and its partial time derivative:

$$\mathbf{B} = \nabla \times \nabla \times \beta\hat{\mathbf{z}} + \nabla \times J\hat{\mathbf{z}} \quad (1)$$

$$\dot{\mathbf{B}} = \nabla \times \nabla \times \dot{\beta}\hat{\mathbf{z}} + \nabla \times \dot{J}\hat{\mathbf{z}} \quad (2)$$

One can then derive these Poisson equations relating the time derivative of the observed magnetic field **B** to corresponding time derivatives of the potential functions:

$$\nabla_h^2 \dot{\beta} = -\dot{\mathrm{B}}_z \quad (3);$$

$$\nabla_h^2 \dot{\mathrm{J}} = -\frac{4\pi \dot{J}_z}{c} = -\hat{\mathbf{z}} \cdot (\nabla_h \times \dot{\mathbf{B}}_h) \quad (4);$$

$$\nabla_h^2 \left(\frac{\partial \dot{\beta}}{\partial z} \right) = \nabla_h \cdot \dot{\mathbf{B}}_h \quad (5)$$

Since the time derivative of the magnetic field is equal to -c∇xE, we can immediately relate the curl of E and E itself to the potential functions determined from the 3 Poisson equations:

Relating ∇xE and E to the 3 potential functions:

$$\nabla \times \mathbf{E} = \frac{-1}{c}\nabla_h\left(\frac{\partial \dot{\beta}}{\partial z}\right) - \frac{1}{c}\nabla_h \times \dot{\mathsf{J}}\hat{\mathbf{z}} + \frac{1}{c}\nabla_h^2 \dot{\beta}\hat{\mathbf{z}} \quad (6)$$

$$\mathbf{E} = \frac{-1}{c}\left(\nabla_h \times \dot{\beta}\hat{\mathbf{z}} + \dot{\mathsf{J}}\hat{\mathbf{z}}\right) - \nabla\psi = \mathbf{E}^{\mathsf{I}} - \nabla\psi \quad (7)$$

The expression for **E** in equation (7) is obtained simply by uncurling equation (6). Note the appearance of the 3-d gradient of an unspecified scalar potential ψ.

The induction equation can be written in component form to illustrate precisely where the depth derivative terms $\partial E_y/\partial z$ and $\partial E_x/\partial z$ occur:

$$\frac{\partial B_x}{\partial t} = c\left(\frac{\partial E_y}{\partial z} - \frac{\partial E_z}{\partial y}\right) = \frac{\partial}{\partial x}\frac{\partial \dot{\beta}}{\partial z} + \frac{\partial \dot{\mathsf{J}}}{\partial y}$$

$$\frac{\partial B_y}{\partial t} = c\left(\frac{\partial E_z}{\partial x} - \frac{\partial E_x}{\partial z}\right) = \frac{\partial}{\partial y}\frac{\partial \dot{\beta}}{\partial z} - \frac{\partial \dot{\mathsf{J}}}{\partial x}$$

$$\frac{\partial B_z}{\partial t} = c\left(\frac{\partial E_x}{\partial y} - \frac{\partial E_y}{\partial x}\right) = -\nabla_h^2 \dot{\beta}.$$

Does it work?

First test: From $\partial B_x/\partial t$, $\partial B_y/\partial t$,$\partial B_z/\partial t$ computed from Bill's RADMHD simulation of the Quiet Sun, solve the 3 Poisson equations with boundary conditions as described, and then go back and calculate $\partial \mathbf{B}/\partial t$ from equation (12) and see how well they agree. Solution uses Newton-Krylov technique:

$\partial B_x/\partial t$ RADMHD

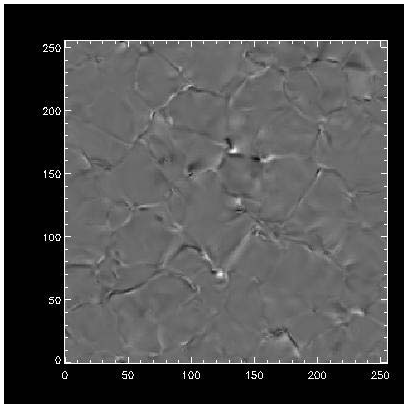

$\partial B_y/\partial t$ RADMHD

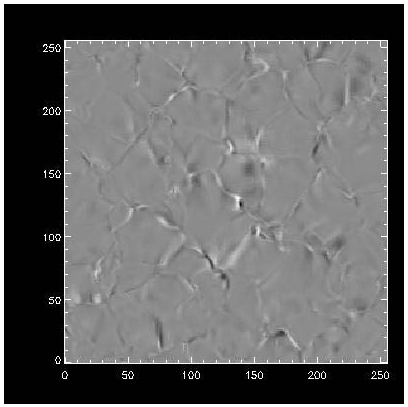

$\partial B_z/\partial t$ RADMHD

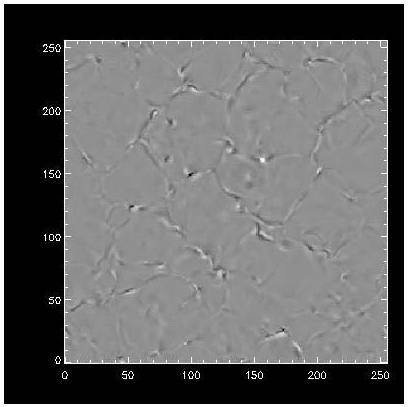

$\partial B_z/\partial t$ vs $\partial B_z/\partial t$

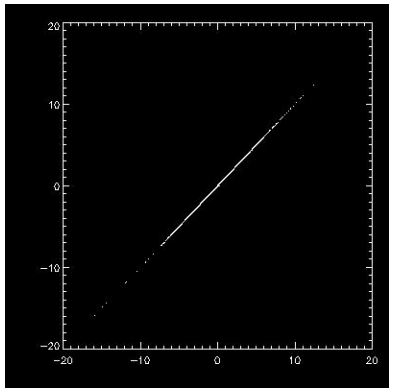

$\partial B_x/\partial t$ derived

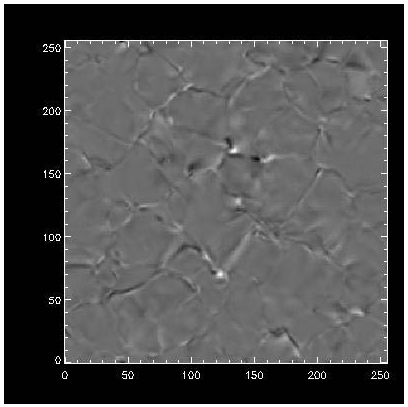

$\partial B_y/\partial t$ derived

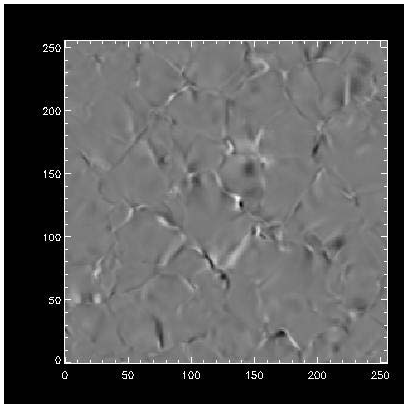

$\partial B_z/\partial t$ derived

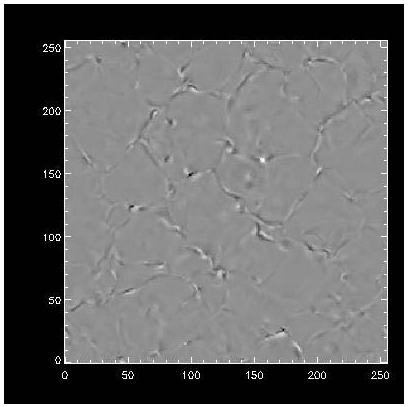

$\partial B_x/\partial t$ vs $\partial B_x/\partial t$

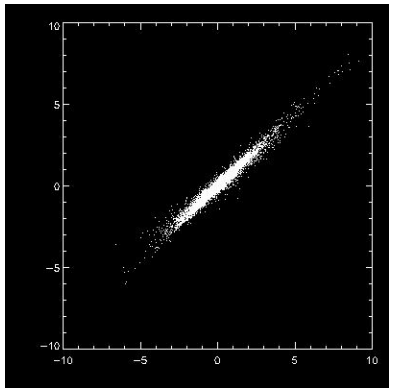

Comparison to velocity shootout case:

$\partial B_x/\partial t$ ANMHD

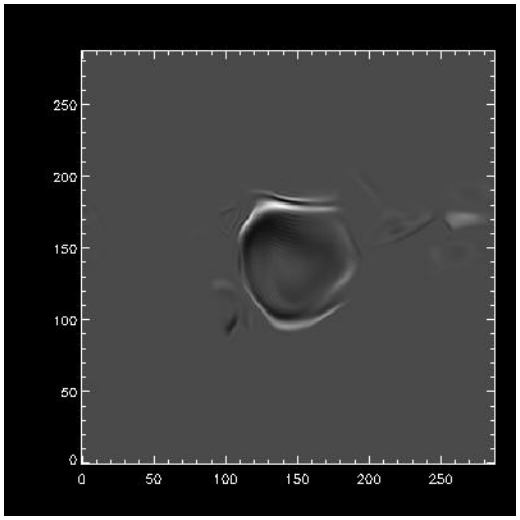

$\partial B_y/\partial t$ ANMHD

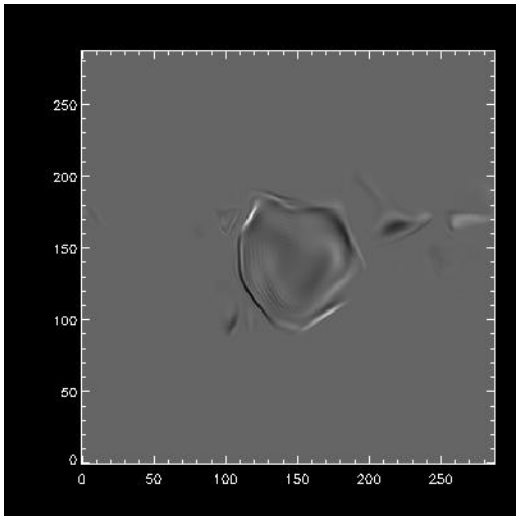

$\partial B_z/\partial t$ ANMHD

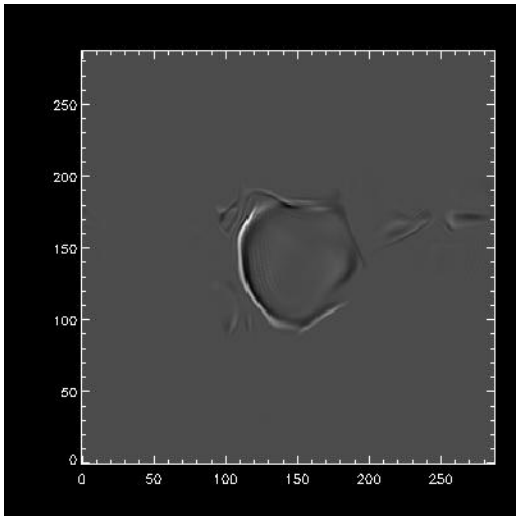

$\partial B_x/\partial t$ derived

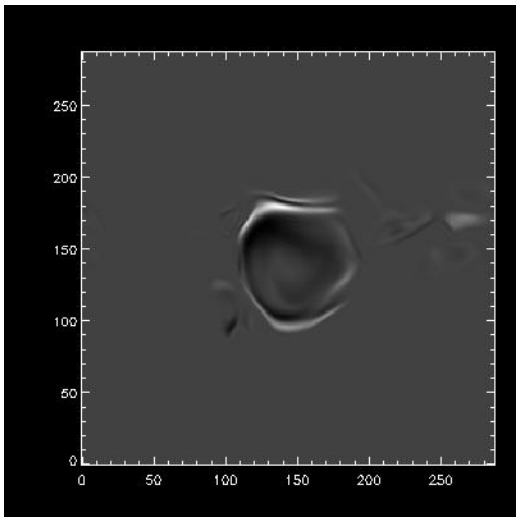

$\partial B_y/\partial t$ derived

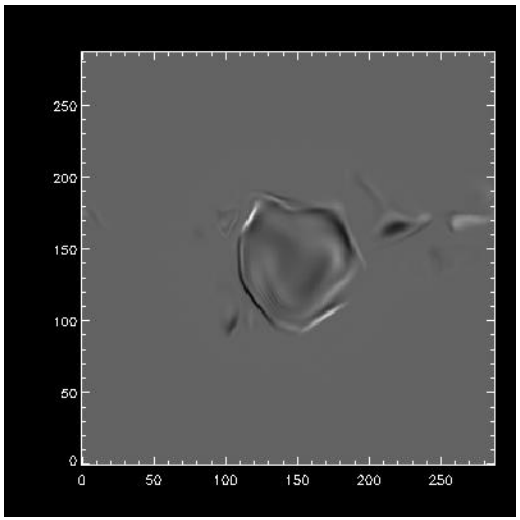

$\partial B_z/\partial t$ derived

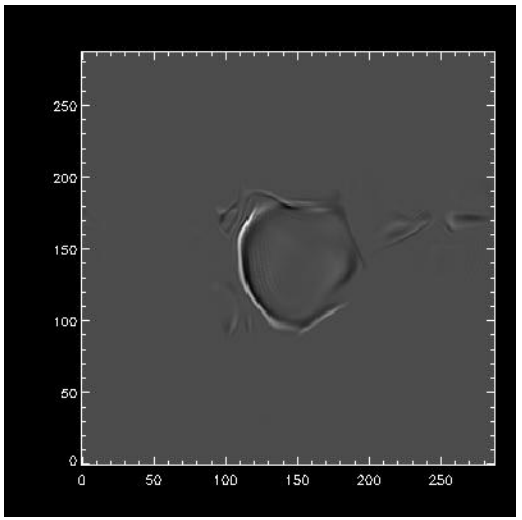

Velocity shoot out case (cont'd)

E_x

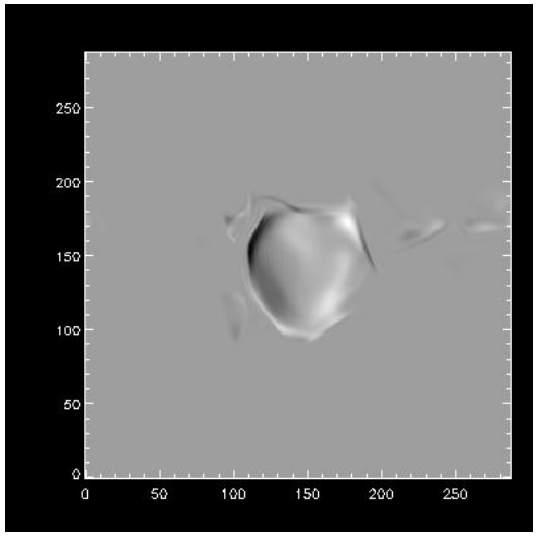

E_y

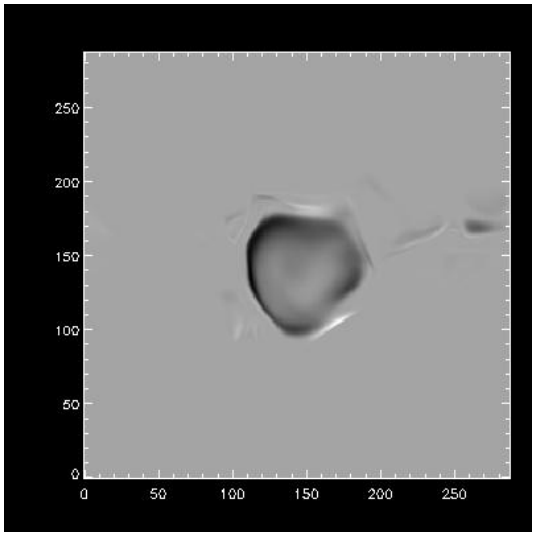

E_z

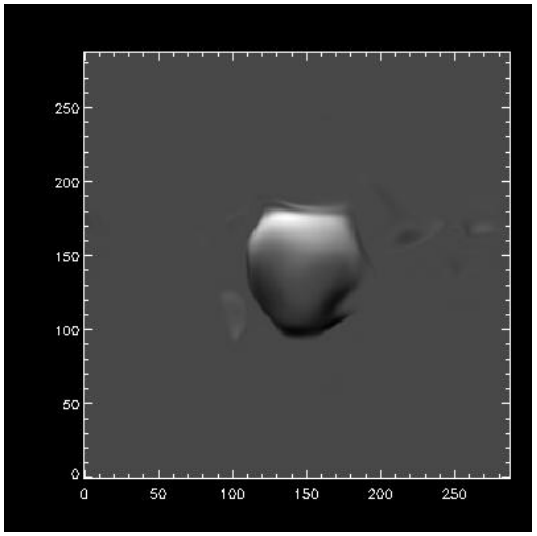

E_x derived

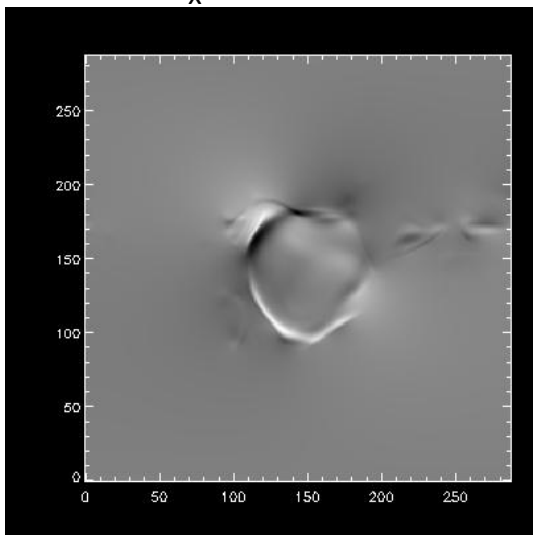

E_y derived

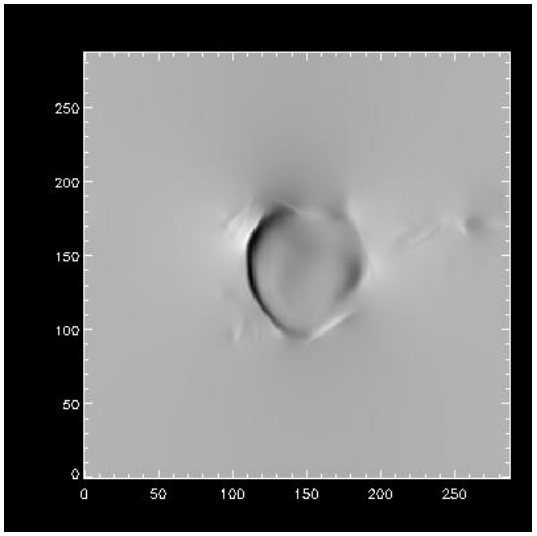

E_z derived

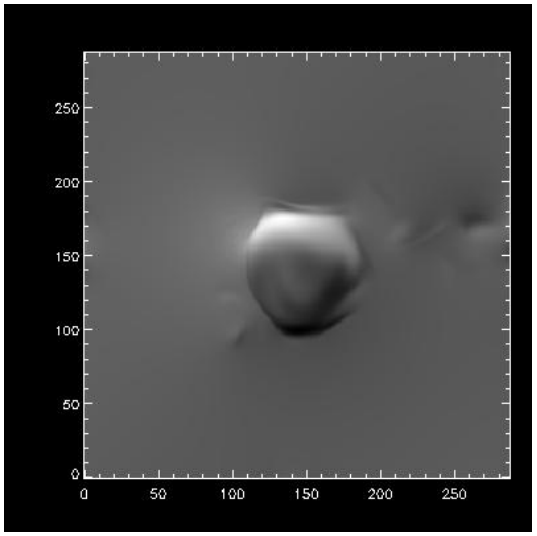

Summary: excellent recovery of ∇xE, only approximate recovery of E.

Why is this? The problem is that **E**, in contrast to ∇**xE**, is mathematically under-constrained. The gradient of the unknown scalar potential in equation (13) does not contribute to ∇**xE**, but it does contribute to **E**.

In the two specific cases just shown, the actual electric field originates largely from the ideal MHD electric field **–v**/c x **B**. In this case, **E**·**B** is zero, but the recovered electric field contains significant components of **E** parallel to **B**. The problem is that the physics necessary to uniquely derive the input electric field is missing from the PTD formalism. To get a more accurate recovery of **E**, we need some way to add some knowledge of additional physics into a specification of $\nabla\psi$.

We will now show how simple physical considerations can be used to derive constraint equations for ψ.

One Approach to finding ψ: A Variational Technique

The electric field, or the velocity field, is strongly affected by forces acting on the solar atmosphere, as well as by the strong sources and sinks of energy near the photosphere. Here, with only vector magnetograms, we have none of this detailed information available to help us resolve the degeneracy in E from $\nabla\psi$.

One possible approach is to vary ψ such that an approximate Lagrangian for the solar plasma is minimized. The Lagrangian for the electromagnetic field itself is E^2-B^2, for example. The contribution of the kinetic energy to the Lagrangian is ½ ρv^2, which under the assumption that **E** = -**v**/c x **B**, means minimizing E^2/B^2. Since B is already determined from the data, minimizing the Lagrangian essentially means varying ψ such that E^2 or E^2/B^2 is minimized. Here, we will allow for a more general case by minimizing W^2E^2 integrated over the magnetogram, where W^2 is an arbitrary weighting function.

A variational approach (cont'd)

$$\min \iint dx\,dy W^2 \left((E_x^I - \frac{\partial \psi}{\partial x})^2 + (E_y^I - \frac{\partial \psi}{\partial y})^2 + (E_z^I - \frac{\partial \psi}{\partial z})^2 \right)$$

$$\equiv \min \iint dx\,dy\; L(x,y) \quad (8)$$

Here the x,y,z components of E^I are assumed to be taken from equation (7) without the $\nabla\psi$ contribution.

To determine $\partial\psi/\partial z$ contribution to the Lagrangian functional, we can use the relationship **E·B**=**R·B** where **R** is any non-ideal contribution to **E**. Performing the Euler-Lagrange minimization of equation (8) results in this equation:

$$\frac{\partial}{\partial x}\frac{\partial L}{\partial\left(\frac{\partial \psi}{\partial x}\right)} + \frac{\partial}{\partial y}\frac{\partial L}{\left(\frac{\partial \psi}{\partial y}\right)} = 0 \quad (9)$$

A variational approach (cont'd)

Evaluating the equation explicitly results in this elliptic 2nd order differential equation for ψ:

$$\nabla_h \cdot W^2\left((\mathbf{E}_h^I - \nabla_h\psi) + \mathbf{B}_h(\mathbf{B}_h \cdot (\mathbf{E}_h^I - \nabla_h\psi) - \mathbf{R}\cdot\mathbf{B})/B_z^2\right) = 0 \qquad (10)$$

We have been pursuing numerical solutions of this equation, along with the 3 Poisson equations described earlier. Comparisons with the original ANMHD electric fields have been poor thus far. This may be due to numerical problems associated with the large dynamic range of the magnetic field-dependent coefficients in this equation.

A more promising approach was recently suggested by Brian Welsch. Writing $E_h = E_h^I - \nabla_h\psi$, and noting that $E_z B_z = \mathbf{R}\cdot\mathbf{B} - \mathbf{B_h}\cdot\mathbf{E_h}$, equation (10) can be re-written and simplified as

$$\nabla_h \cdot \left((W^2/B_z)(\boldsymbol{E}\times\boldsymbol{B})\times\hat{\boldsymbol{z}}\right) = 0 \qquad (11)$$

or

$$\hat{\boldsymbol{z}}\cdot\left(\nabla_h \times ((W^2/B_z)\boldsymbol{E}\times\boldsymbol{B})\right) = 0. \qquad (12)$$

A variational approach (cont'd)

Equation (12) implies that we can write

$$(W^2/B_z)(c\mathbf{E}\times\mathbf{B})_h = (W^2/B_z)(c\mathbf{E_h}\times B_z\hat{\mathbf{z}} + cE_z\hat{\mathbf{z}}\times\mathbf{B_h}) = -\nabla_h\chi \quad (13)$$

Dividing by W^2 and then taking the divergence of this equation, we derive an elliptic equation for χ that involves the magnetic field or its time derivatives:

$$\frac{\partial B_z}{\partial t} + \nabla_h\cdot\left(\frac{c\mathbf{R}\cdot\mathbf{B}}{B^2}\hat{\mathbf{z}}\times\mathbf{B}_h\right) +$$

$$\nabla_h\cdot\left(\frac{(\mathbf{B_h}\cdot\nabla_\mathbf{h}\chi)}{W^2B^2}\mathbf{B}_h\right) = -\nabla_h\cdot\left(\frac{B_z^2\nabla_h\chi}{W^2B^2}\right) \quad (14)$$

A variational approach (cont'd)

If the non-ideal part of the electric field R is known or if one desires to specify how it varies over the magnetogram field of view, equation (14) can incorporate non-ideal terms in its solution. However, we anticipate that most of the time, the non-ideal term will be much smaller than ideal contributions, and can be set to 0.

Once χ has been determined, it is straightforward to derive the electric field and the Poynting flux **S**=(c/4π)**E**x**B**:

$$\frac{cE_z}{B_z} = \frac{c\mathbf{R}\cdot\mathbf{B}}{B^2} - \frac{\nabla_h\chi\cdot\mathbf{z}\times\mathbf{B_h}}{W^2B^2} \quad (15)$$

$$c\mathbf{E_h} = \frac{c\mathbf{R}\cdot\mathbf{B}}{B^2}\mathbf{B}_h - \frac{B_z^2}{W^2B^2}\hat{\mathbf{z}}\times\nabla_h\chi - \frac{\mathbf{B_h}\cdot\nabla_\mathbf{h}\chi}{W^2B^2}\hat{\mathbf{z}}\times\mathbf{B}_h \quad (16)$$

$$\mathbf{S}_h = -\frac{B_z}{4\pi W^2}\nabla_h\chi \quad (17); \quad S_z = \frac{\nabla_h\chi\cdot\mathbf{B_h}}{4\pi W^2} \quad (18)$$

A variational approach (cont'd)

Finally, if one can ignore the non-ideal **R•B** term in equation (14), then the two special cases of $W^2B^2=1$(minimized kinetic energy) and $W^2=1$ (minimized electric field energy) result in these simplified versions of equation (14) for χ:

$$(W^2B^2=1:)\quad \nabla_h\cdot\left(B_z^2\nabla_h\chi\right)+\nabla_h\cdot\left(\left(\mathbf{B_h}\cdot\nabla_h\chi\right)\mathbf{B_h}\right)=\frac{\partial B_z}{\partial t}\qquad(19)$$

$$(W^2=1:)\quad \nabla_h\cdot\left(b_z^2\nabla_h\chi\right)+\nabla_h\cdot\left(\left(\mathbf{b_h}\cdot\nabla_h\chi\right)\mathbf{b_h}\right)=\frac{\partial B_z}{\partial t}\qquad(20)$$

Boundary conditions for χ are not clear, but if the outer boundary of the magnetogram has small or zero magnetic field values, it is likely that the horizontal Poynting flux, and hence $\nabla_h\chi$, has a small flux normal to the magnetogram boundary. Therefore we anticipate that Neumann boundary conditions are the most appropriate for applying to χ if the boundaries are in low field-strength regions.

Note that once χ has been solved for, the potential field contribution can be found by subtracting the PTD solutions for E^I from the electric field from equations (15-16).

A Variational Approach (cont'd)

S_x

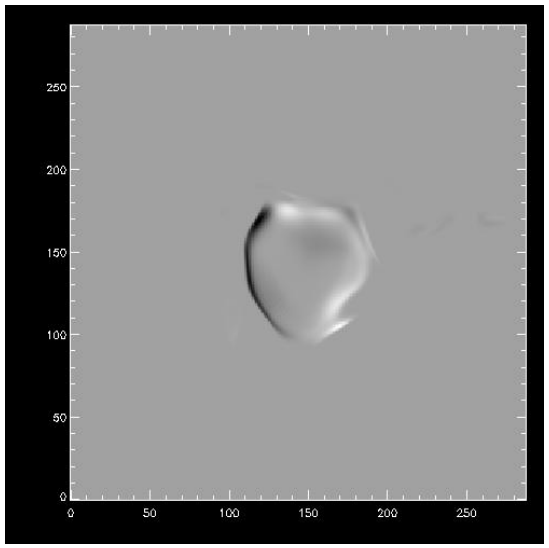

S_y

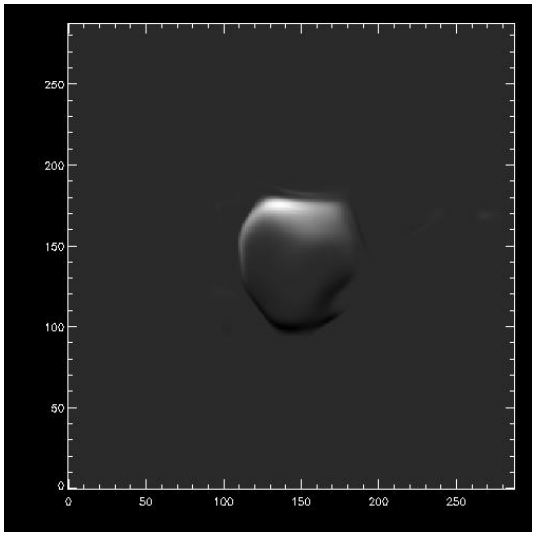

S_z

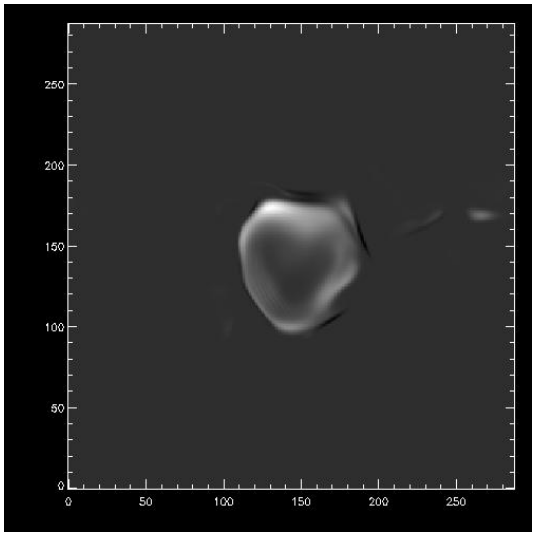

S_x (var)

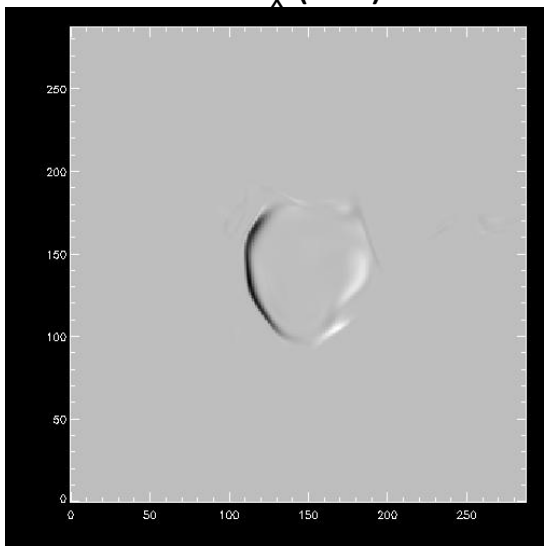

S_y (var)

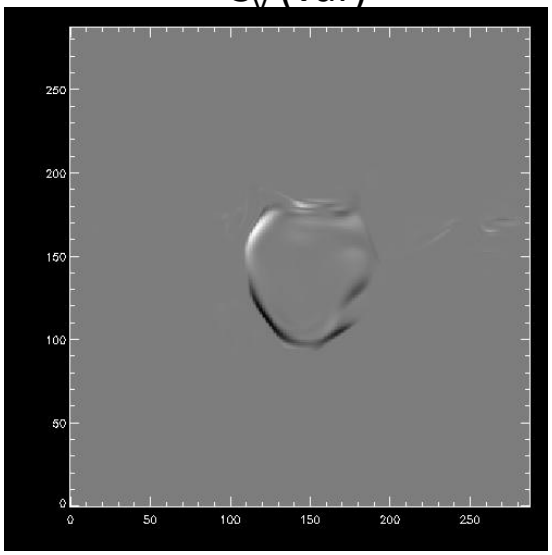

S_z (var)

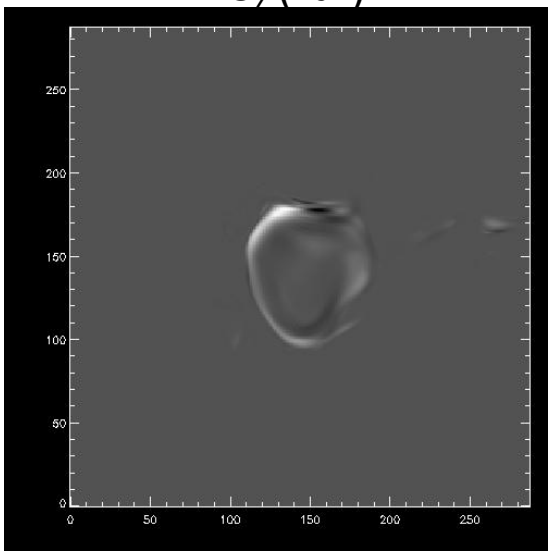

Summary of 3D electric field inversion

• It is possible to derive a 3D electric field from a time sequence of vector magnetograms which obeys all components of the Maxwell Faraday equation. This formalism uses the Poloidal-Toroidal Decomposition (PTD) formalism.

•The PTD solution for the electric field is not unique, and can differ from the true solution by the gradient of a potential function. The contribution from the potential function can be quite important.

•An equation for a potential function, or for a combination of the PTD electric field and a potential function, can be derived from variational principles and from iterative techniques.

•The development and testing of numerical techniques are currently underway.